Effects of calcination temperature on the photocatalytic activity and photo-induced super-hydrophilicity of mesoporous TiO_2 thin films

Jiaguo Yu,[a,b] Jimmy C. Yu,*[a] Wingkei Ho[a] and Zitao Jiang[a]

[a] *Department of Chemistry and Materials Science and Technology Research Centre The Chinese University of Hong Kong, Shatin, New Territories, Hong Kong, China. E-mail: jimyu@cuhk.edu.hk*

[b] *State Key Laboratory of Advanced Technology for Materials Synthesis and Processing Wuhan University of Technology, Wuhan 430070 China*

Received (in London, UK) 25th January 2002, Accepted 15th February 2002
First published as an Advance Article on the web 9th April 2002

Mesoporous TiO_2 nanometer thin films were prepared on fused quartz by the dip-coating sol–gel method from a system containing a triblock copolymer as a template (or pore-forming agent), and then calcined at different temperatures. These films were characterized by X-ray diffraction, atomic force microscopy, X-ray photoelectron spectroscopy, BET surface area and UV-visible spectrophotometry. The photocatalytic activity and photo-induced super-hydrophilicity of the films were evaluated by the photocatalytic degradation of acetone and water contact angle measurement in air, respectively. It was found that the thin films calcined at 700 °C not only show the highest photocatalytic activity, but also possess the greatest light-induced hydrophilicity and the slowest conversion rate from the hydrophilic to a hydrophobic state. The former is attributed to the fact that the films calcined at 700 °C are composed of anatase and rutile, whichis beneficial in enhancing the transfer of photo-generated electrons from the anatase to the rutile phase, reducing the electron–hole combination rate in anatase and enhancing its activity. The high light-induced hydrophilicity and slow hydrophilic to hydrophobic conversion rate are due to the synergetic effect of good photocatalytic activity, sufficient surface hydroxyl content and a degree of surface roughness. Because of their high specific surface areas and mesoporous structures, the photocatalytic activity of mesoporous TiO_2 thin films is higher than that of conventional TiO_2 thin films.

Porous materials have attracted more and more attention in the fields of separation and catalysis owing to their high specific areas and pore volumes, as well as their narrow pore size distributions. Mesoporous materials were first synthesized by Mobil researchers in 1992,[1,2] and have played an important role in both basic and applied research areas in recent years. Many metal oxides, especially porous ones, have special catalytic functions.[3–8] Titania has been widely used as a catalyst in organic reactions such as selective oxidation and photocatalytic reactions such as alcohol dehydration, photo-Kolbe oxidations of organic acids,[9] oxidation of aromatic compounds,[10] degradation of paint pigments[11] and nitrogen oxide reduction.[12] Mesoporous titania should be an even more effective catalyst because of its large surface area and porosity. Mesoporous titania (Ti-TMS1) was first synthesized through modified sol–gel routes in the presence of alklyphosphate surfactant templates by Antonelli and Ying in 1995.[5] Since then, numerous research papers on synthetic methods and catalytic properties have appeared.[6–8,13–19] Recent investigations have confirmed that block polymers could also be used as templates to direct the formation of mesoporous titania and other oxides.[6–8] Very recently, we have also reported methods for the preparation of mesoporous TiO_2 thin films and powders by reverse micelle synthesis and ultrasonic illumination.[20–23]

In the present work, we employ a triblock copolymer as a template (or pore-forming agent), which is known to be effective in the synthesis of mesoporous titania materials.[24,25] The mesoporous TiO_2 thin films were prepared by a dip-coating sol–gel method using acetylacetone as a complexing agent. The obtained TiO_2 thin films were then calcined at different temperatures. This is the first report on the effects of calcination temperature on the surface microstructures, photocatalytic activity and photo-induced hydrophilic properties of sol–gel-derived mesoporous TiO_2 thin films from a system containing a triblock copolymer template.

Experimental

Preparation

All chemicals used in the present work were from Aldrich and were used as received. Millipore water was used in all experiments.

Titanium tetraisopropoxide (TTIP) was used as the titanium source. 0.1 mol TTIP was dissolved slowly in 182 ml absolute ethanol under vigorous stirring. 0.1 mol acetylacetone and 0.1 mol water were then added to the alcohol solution, followed by 20 g of a triblock copolymer: $HO(CH_2CH_2O)_{20}\{CH_2CH(CH_3)O\}_{70}(CH_2CH_2O)_{20}H$ (average molecular weight *ca.* 4400, designated $EO_{20}PO_{70}EO_{20}$, P_{123}). The mixture was stirred for 1 h to dissolve the P_{123} completely. The solution appeared transparent with a light yellow–orange colour. Quartz (80 mm × 30 mm × 2mm) was used as the substrate for the thin films. The TiO_2thin films were prepared by the dip-coating sol–gel method. The withdrawal speed was 3 mm s^{-1}. Wet gel thin films were dried at 100 °C for 30 min and then heat treated at a rising rate of 3 °C min^{-1} up to 500 °C, and kept at that temperature for 1 h in air. The template P_{123} contained in the gel coating films decomposed completely at

500 °C. After calcination at 500 °C, the thin films were again heat treated at 700 and 900 °C for 1 h.

Apart from the above-described thin film samples, powder samples were also prepared. TiO_2 sols with the same compositions as the thin film samples were dried at 100 °C in air in order to obtain gels. The gels were then heat treated at a heating rate of 3 °C min^{-1} to 500 °C, and kept at that temperature for 1 h in air. The dried samples were ground in an agate mortar to obtain TiO_2 powders. Finally, the prepared TiO_2 powders were again calcined at 700 and 900 °C for 1 h.

Characterization

The surface roughness and morphology of the mesoporous TiO_2 thin films were evaluated by atomic force microscopy (AFM) using a Digital Instruments Nano Scope 3a instrument. The X-ray diffraction (XRD) patterns, obtained on a Philips MPD 18801 X-ray diffractometer using Cu-Kα radiation at a scan rate of 0.05° S^{-1} in 2θ, were used to determine the identity of any phases present, the phase composition and their crystallite size. The accelerating voltage and the applied current were 35 kV and 20 mA, respectively. Crystallite size was calculated from X-ray line broading analysis by the Scherrer formula. UV-Vis spectra of films were obtained using a Varian Cary 100 Scan UV-visible spectrophotometer. X-Ray photoelectron spectroscopy (XPS) measurements were performed on a PHI Quantum 2000 XPS system with a monochromatic Al-Kα source and a charge neutralizer; all the binding energies were referenced to the C1s peak of adventitious surface carbon at 284.8 eV. Film thickness was measured using a Tencor Instruments Alpha-step 500 surface profiler. The Brunauer–Emmett–Teller (BET) surface areas (S_{BET}) and pore parameters of the powder samples were determined by nitrogen adsorption–desorption isotherm measurements at 77 K on a Micromeritics ASAP 2000 nitrogen adsorption apparatus. All the samples measured were degassed at 180 °C before the actual measurements. Pore size distributions were calculated from the desorption branch of the isotherm by the Barrett–Joyner–Halenda (BJH) method using the Halsey equation.[26]

Measurement of photoactivity and water contact angle

The photocatalytic activity of mesoporous TiO_2 thin films for the degradation of acetone in air was performed at ambient temperature using a 7000 ml reactor. The experimental process has been described in detail in our previous papers.[20] Each photocatalytic reaction was followed for 60 min. The measurements were repeated for each catalytic system, and the experimental error was found to be within ±3%. The photocatalytic oxidation of acetone is a pseudo-first-order reaction and its kinetics may be expressed as[20,27] $\ln(C_0/C) = kt$, where k is the apparent pseudo-first-order rate constant, and C_0 and C are the initial and reaction concentrations of acetone, respectively.

Water contact angles on the surface of mesoporous TiO_2 thin films were measured with a Kyowa CA-X contact angle meter by the sessile drop method. The experimental error for the measurements is ±1°. The droplet size used for the measurements was 3 μL. Water droplets were placed at five different positions for each sample and the average value was adopted as the contact angle. The water contact angles (θ) for the freshly prepared TiO_2 thin films at different temperatures were about 10–15°. However, when these samples were stored in the dark for 3 months, the water contact angles increased to about 60°. When illuminated by a 15 W 365 nm UV lamp (Cole-Parmer Instrument Co.), the water contact angles of the films dropped steadily to below 5°. The integrated UV intensity in the range 310–400 nm striking the films, measured with a UVP UVX UV radiometer, was 540 ± 10 μW cm^{-2}. The hydrophilic and hydrophobic properties of the TiO_2 thin films were characterized by examining the change in the water contact angle under UV illumination and in the dark.

Results and discussion

Characterization

Fig. 1 shows the transmittance of quartz and of the mesoporous TiO_2 thin films deposited on quartz by 1 coating cycle and calcined at 500, 700 and 900 °C. The changes in the transmittance spectra and absorption edge wavelength of TiO_2 films calcined at different temperatures are attributed to differences in film thickness (as shown in Table 1), surface microstructure and absorption of light. TiO_2 films calcined at 500 and 700 °C have the highest transmittance, >78% over the entire visible light region. The fast decay below 380 nm is due to absorption of light caused by the excitation of electrons from the valence band to the conduction band of TiO_2. However, in the case of the film calcined at 700 °C, the absorption edge wavelength of TiO_2 shows a slight pseudo-"red shift". This is ascribed to the fact that the TiO_2 film calcined at 700 °C contains larger TiO_2 grains compared to the film calcined at 500 °C, with a certain amount of rutile. After calcination at 900 °C, the transmittance of the film decreases greatly and the absorption edge wavelength shows a significant "red shift". This is because TiO_2 film calcined at 900 °C is purely rutile, which has a more intense absorbance and a smaller bandgap than anatase. The films calcined at 500, 700 and 900 °C have thicknesses of about 150, 130 and 120 nm, respectively.

The difference in absorption edge wavelength for the TiO_2 thin films clearly indicates a decrease in the bandgap of TiO_2 with increasing heat treatment temperature. In order to obtain a quantitative estimate of the bandgap energies, the absorption coefficient (α) of the films, near the absorption edge, was calculated from the transmittance (T) and reflectance (R) data using the simplified relation $T = (1-R)^2e^{-\alpha d}/(1-R^2e^{-2\alpha d})$, where d is the thickness of the films.[28–30] The intercepts of the tangents to the $(\alpha h\nu)^{1/2}$ *versus* photon energy ($h\nu$) plots give estimates of the bandgap energies of TiO_2. Plots of $(\alpha h\nu)^{1/2}$ *versus* photon energy ($h\nu$) drawn for the TiO_2 films calcined at 500, 700 and 900 °C are shown in Fig. 2. The bandgap energies estimated from the intercepts of the tangents to the plots are about 3.3, 3.2 and 3.0 eV for TiO_2 films calcined at 500, 700 and 900 °C, respectively. Our results are in good agreement with the values reported in the literature.[28,31]

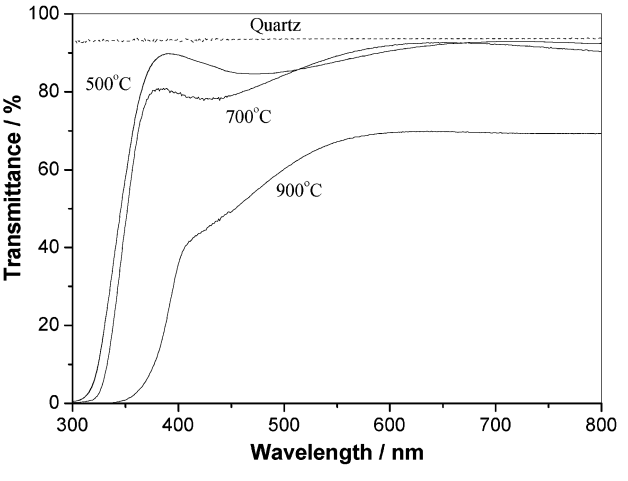

Fig. 1 Transmittance of quartz and of mesoporous TiO_2 thin films deposited on quartz by 1 coating cycle and calcined at 500, 700 and 900 °C.

Table 1 Physicochemical properties of mesoporous TiO_2 films calcined at different temperatures[a]

Calcination temp./°C	Thickness/μm	Phase structure	Phase composition[b]	Crystallite size/nm	R_{rms}/nm	%OH (before UV)	%OH (after UV)
500	0.15	A	A: 100%	12.3	1.53	11.3	18.9
700	0.13	A and R	A: 77%	A: 33.6	2.47	10.6	16.3
			R: 23%	R: 50.6			
900	0.12	R	R: 100%	59.6	4.53	6.3	11.1

[a] All film samples deposited on quartz by 1 coating cycle. [b] A: anatase, R: rutile.

Fig. 3 shows the XRD patterns of mesoporous TiO_2 films deposited on quartz and calcined at 500, 700 and 900 °C. The TiO_2 films calcined at 500 and 900 °C exhibit anatase and rutile phase structures, respectively. It is obvious that the anatase and rutile TiO_2 films exhibit preferential orientation in the (101) and (110) peaks, respectively. The mesoporous TiO_2 thin film calcined at 700 °C is composed of anatase and rutile. The average crystallite size and phase composition of the TiO_2 films, shown in Table 1, were calculated according to ref. 22 and 32.

Fig. 4 shows two- and three-dimensional AFM images of the surface of the mesoporous TiO_2 thin films. It was observed that, at different heat treatment temperature, the surface morphologies and roughness of the mesoporous TiO_2 films are obviously different. The film calcined at 500 °C has a granular microstructure and a flat texture, with the lowest surface roughness of the three, and is composed of mono-dispersed spherical particles of about 70–80 nm in diameter. According to previous XRD results, these 70–80 nm particles on the surface of TiO_2 thin films are aggregates of many small TiO_2 crystallites.[20] In addition to particle diameter, AFM image analysis also gives the values for the surface roughness. The root mean square roughness value (R_{rms}) of mesoporous TiO_2 calcined at 500 °C is 1.53 nm, as shown in Table 1.

With increasing calcination temperature, the surface morphology and roughness of the mesoporous TiO_2 films changed significantly owing to the phase transformation of anatase to rutile and sintering and growth of TiO_2 crystallites. Fig. 4(c and d) show that the mesoporous TiO_2 film heat treated at 700 °C is composed of *ca.* 160 nm spherical particles. However, after calcination at 900 °C, the diameter of the TiO_2 particles is smaller (about 140 nm), probably due to sintering of the particles and the difference in phase structure (or density), as shown in Fig. 4(e and f). Table 1 shows that the roughness values increase with increasing calcination temperature.

The BET surface areas of mesoporous TiO_2 thin films could not be measured directly by nitrogen adsorption apparatus, because the amount of the thin films on quartz was too small. We measured the BET surface areas of powder samples prepared through the same procedure as the thin films. Fig. 5 shows Barrett–Joyner–Halenda (BJH) pore size distribution plots for mesoporous TiO_2 powder calcined at 500 °C for 1 h and nitrogen sorption isotherms that are typical of mesoporous TiO_2. Such strong hysteresis is believed to be related to the capillary condensation associated with pore channels and/or cages.[25] The BJH analyses show that the calcined mesoporous TiO_2 powder exhibits a mean pore size of 5.04 nm and a narrow pore size distribution (2.7–6.2 nm). The BET surface areas and pore parameters of the mesoporous TiO_2 powders calcined at different temperatures determined from the nitrogen adsorption–desorption isotherms by the BJH method are summarized in Table 2. The pore size distribution curves and nitrogen sorption isotherms of TiO_2 powders calcined at 700 and 900 °C (not shown here) are different from those of the TiO_2 powder heat treated at 500 °C. The BET surface areas decrease significantly with increasing calcination temperature. Moreover, the pore size distribution becomes wider. Table 2 also shows that the porosity and pore volume of the mesoporous TiO_2 powders decrease significantly at higher temperatures.

Fig. 6 shows high resolution XPS spectra of the O1s region for mesoporous TiO_2 films calcined at 500 °C before and after UV illumination. The O1s region is fitted into two peaks (dashed lines). The peaks at 529.90 and 531.90 eV correspond to Ti–O in TiO_2 and hydroxyl groups (–OH), respectively. After UV illumination, the area of the peak due to the hydroxyl groups increases, indicating that the chemisorption of water molecules on the surface of mesoporous TiO_2 films is enhanced by UV irradiation. The increase in hydroxyl content may lead to the formation of super-hydrophilic TiO_2 surfaces. Table 1 lists the changes in hydroxyl content on the surface of mesoporous TiO_2 films calcined at different temperature before and after UV illumination. The hydroxyl content (%) is the

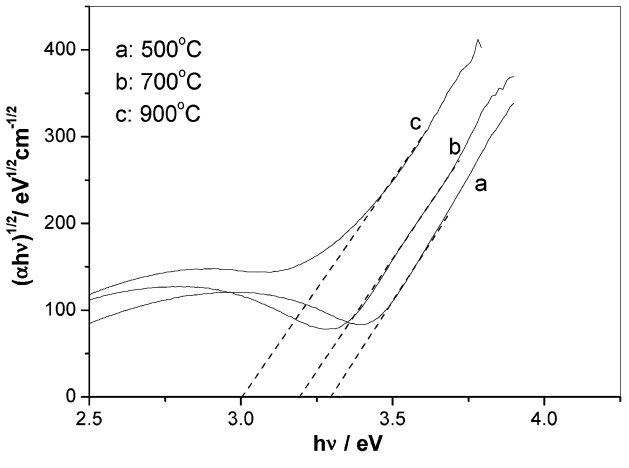

Fig. 2 Plots of $(\alpha h\nu)^{1/2}$ *versus* $h\nu$ for the mesoporous TiO_2 thin films calcined at (a) 500, (b) 700 and (c) 900 °C.

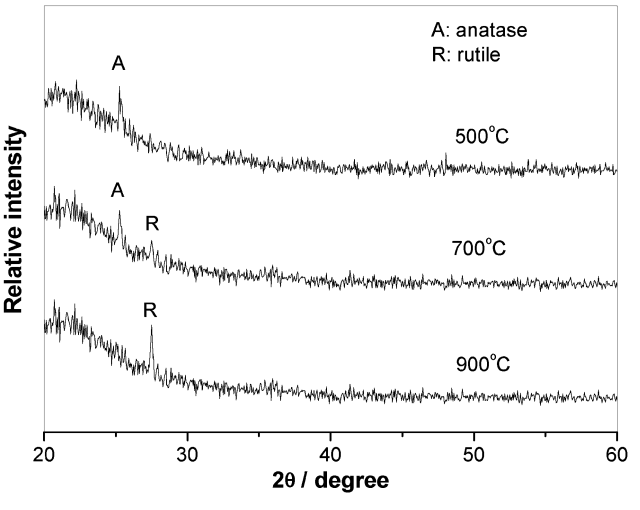

Fig. 3 XRD patterns of mesoporous TiO_2 films heat treated at (a) 500, (b) 700 and (c) 900 °C.

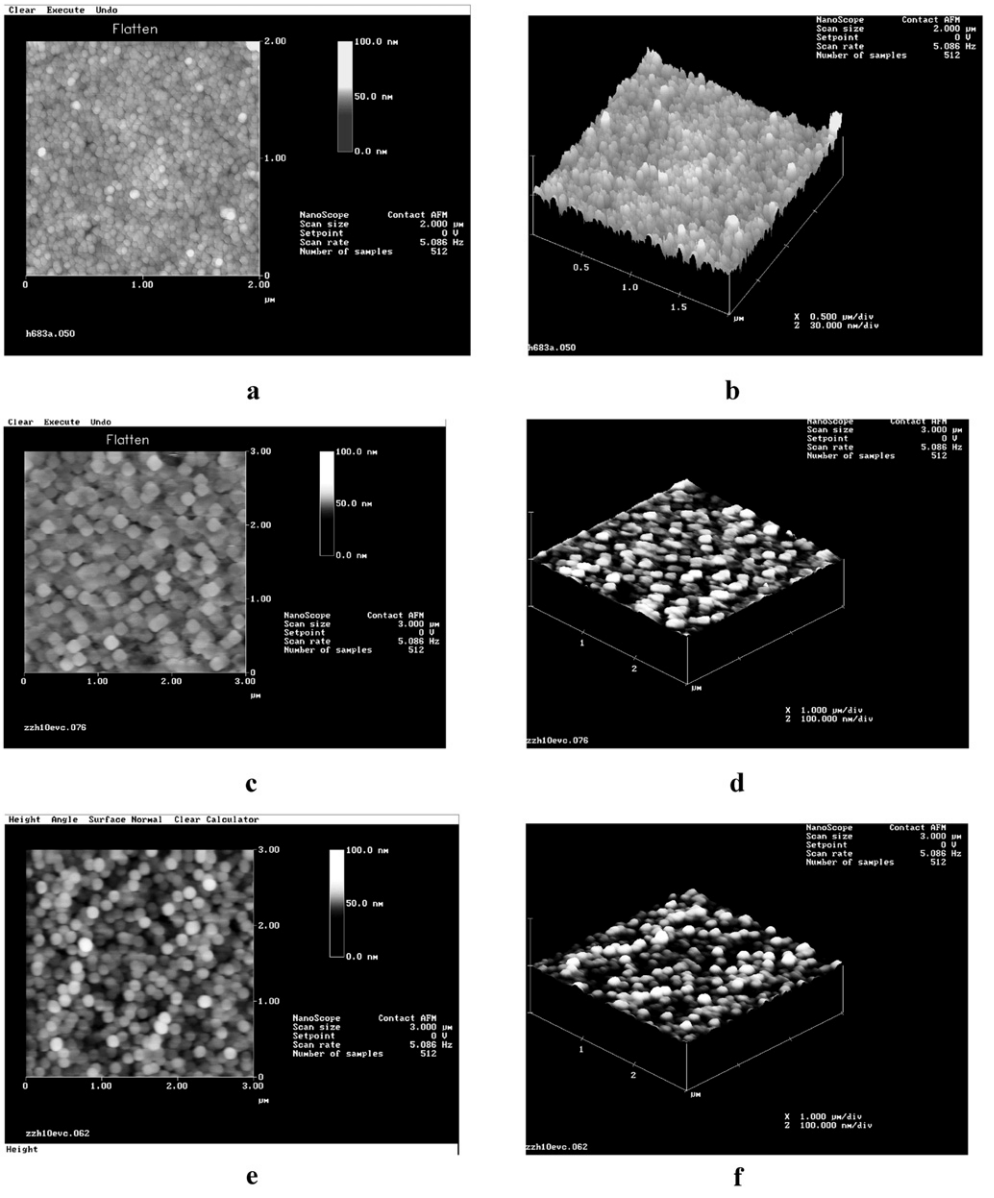

Fig. 4 Two- and three-dimensional AFM images of the surface of mesoporous TiO_2 thin films calcined at (a, b) 500, (c, d) 700 and (e, f) 900 °C.

ratio of the area of the 531.90 eV peak to the total area of the two O1s peaks. The hydroxyl contents in all samples after UV illumination are greater than those before UV illumination. This is because some water molecules are dissociatively adsorbed on defective sites on the TiO_2 film surfaces.[33] The hydroxyl groups detected by XPS on the film surfaces are chemisorbed H_2O. Although some H_2O is physically adsorbed on the surface of TiO_2 films, the physisorbed H_2O on TiO_2 is easily desorbed under the ultra-high vacuum condition of the XPS system. Therefore, the XPS spectra do not show physisorbed H_2O on the surface of the TiO_2 films. Table 1 also shows that the hydroxyl content of TiO_2 thin films calcined at 500 and 700 °C is obviously greater than that of TiO_2 thin films heat treated at 900 °C. This is because the former have smaller anatase crystallites and higher specific surface areas. Usually, an increase in the hydroxyl content on the surface of TiO_2 films can enhance the photo-induced super-hydrophilicity and photocatalytic activity.[33–34]

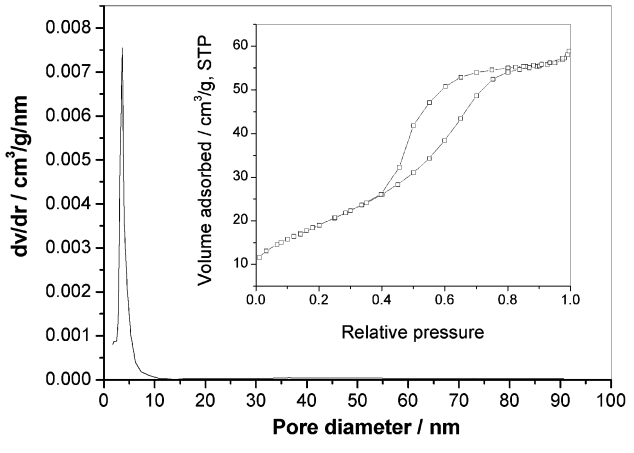

Fig. 5 Pore size distribution curve calculated from desorption branch of the nitrogen isotherm by the BJH method and the corresponding nitrogen adsorption–desorption isotherms (inset) of mesoporous TiO_2 powder calcined at 500 °C for 1 h.

Photocatalytic activity

In order to evaluate the photocatalytic activity of mesoporous TiO_2 thin films prepared by our method, a comparison of the photoactivity of the mesoporous TiO_2 thin films and a conventional TiO_2 thin film was conducted. It can be seen from Table 3 that, at 500 °C, the photocatalytic activity of mesoporous TiO_2 thin films prepared by our method is obviously higher

Table 2 Effects of calcination temperature on BET surface areas and pore parameters of mesoporous TiO_2

Temp./°C	S_{BET}[a] /m^2 g^{-1}	Porosity[b] (%)	Pore volume[c] /ml g^{-1}	Pore size[d] /nm	Pore range/nm
500	69.9	24.6	0.088	5.04	2.7–6.2
700	10.5	10.6	0.032	12.2	3.1–16.4
900	2.7	3.2	0.009	37.3	10.5–101.2

[a] BET surface area calculated from the linear part of the BET plot ($P/P_0 = 0.1$–0.2). [b] The porosity is estimated from the pore volume determined using the adsorption branch of the N_2 isotherm curve at the single point where $P/P_0 = 0.975$. [c] Total pore volume, taken from the volume of N_2 adsorbed at $P/P_0 = 0.975$. [d] Average pore diameter, estimated using the adsorption branch of the isotherm and the Barrett–Joyner–Halenda (BJH) formula.

than that of a TiO_2 thin film prepared by the conventional sol–gel route.[20] The apparent rate constant, degradation rate and specific photocatalytic activity of the mesoporous TiO_2 thin films are greater than those of the conventional TiO_2 film by a factor of about 1.6 times. This is probably due to the large BET specific surface area of the mesoporous samples. The specific surface area of mesoporous TiO_2 can be as high as 69.9 m^2 g^{-1}, while that of the conventional TiO_2 is only 9.1 m^2 g^{-1}, as shown in Table 2 of ref. 20. Furthermore, mesoporous structures may allow more effective diffusion of various gaseous reactants and products during photocatalytic reaction, and thus improve the photocatalytic activity.

The photocatalytic activity of mesoporous TiO_2 films calcined at 700 °C is slightly greater than those treated at the lower temperature. However, Table 2 shows that the BET surface area, porosity and pore volume of mesoporous TiO_2 heat treated at 700 °C is much lower than that calcined at 500 °C. Perhaps the small enhancement in the photocatalytic activity is mainly caused by the changes in the phase structures in the films (as shown in Fig. 3), since calcination at 700 °C accelerates phase transformation from anatase to rutile and the crystallization of anatase. On the basis of our previous results, a composite of two phases of the same semiconductor and good crystallization of anatase both lead to an improvement in photoactivity.[21,22] Thus, the films calcined at 700 °C contain many hetero-junctions between the anatase and rutile phases, owing to the high dispersion of rutile in the films. Fig. 7 shows a schematic illustration of the energy diagram for the heterogeneous anatase/rutile TiO_2 system at pH 7. It has been reported that the band gaps of anatase and rutile TiO_2 are 3.2 and 3.0 eV,[35–37] respectively; also, the flat band potentials of anatase and rutile TiO_2 are about −0.9 and −0.7 V (*versus* normal hydrogen electrode at pH 7),[36] respectively. Therefore, the conduction band of rutile is considered to be lower level than that of anatase. As shown in Fig. 7, the coupling of two phases allows the vectorial displacement of electrons from the anatase phase to the rutile phase and retards the recombination of the electron–hole pairs in anatase.[38] Upon UV excitation, photo-generated electrons accumulate in the lower-lying conduction band of rutile, whereas holes can accumulate in the valence bands of both anatase and rutile, since their valence bands are almost at the same level. Accumulated electrons in the conduction band of rutile can be transferred to oxygen adsorbed on the surface to form O_2^- or O_2^{2-}.[38] Accumulation of holes in the valence band of anatase and rutile leads to the production of surface hydroxyl radicals $^{\bullet}OH$, which are responsible for the oxidation decomposition of acetone. As for the heterogeneous anatase/rutile TiO_2 system, photo-generated electrons are effectively accumulated in the rutile phase, without recombining with the holes in the anatase valence band, which leads to the enhancement of the photocatalytic activity of anatase. Of course, the better crystallinity of anatase in TiO_2 treated at 700 °C is also beneficial to the photocatalytic activity.

As expected, mesoporous TiO_2 films calcined at 900 °C show virtually no photoactivity, as they contain purely the rutile phase.

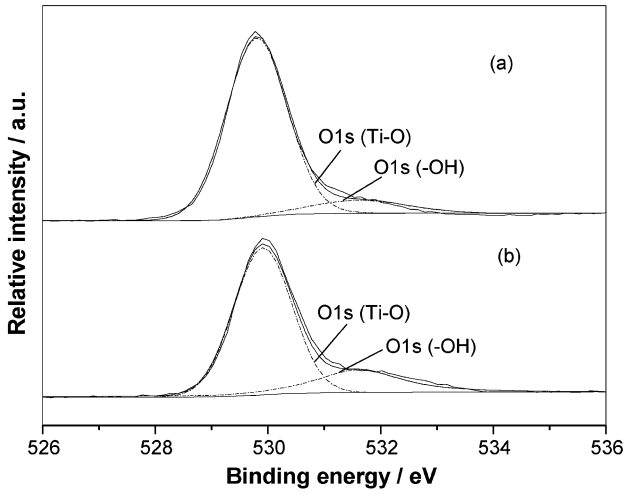

Fig. 6 High resolution XPS spectra of the O1s region of mesoporous TiO_2 thin films calcined at 500 °C before (a) and after (b) UV illumination.

Photo-induced super-hydrophilicity

The as-prepared mesoporous TiO_2 thin films on quartz show low water contact angles of about 10–15°. This can be explained by the clean surface and the surface defect structures of the as-prepared mesoporous TiO_2 thin films.[39] However, when these films were stored in dark rooms in air for three months, the water contact angle tended to increase up to saturation contact angle values of about 50–60°. This is ascribed to the fact that the surface is contaminated by adsorbing some gaseous contaminants from the air and the surface defect sites can be healed or replaced gradually by oxygen atoms, which changes the surface wettability from hydrophilic to hydrophobic.

Fig. 8 shows the changes in water contact angle for mesoporous TiO_2 thin films when illuminated by UV light for 60 min and subsequently stored in a dark room for 7 days. It can be seen that the hydrophobic ↔ hydrophilic inter-conversion rates of the films are obviously different, depending on the temperature at which they were calcined. The surface of all the samples becomes highly hydrophilic with a water contact angle of less than 5° under 540 μW cm^{-2} UV illumination within 60 min. It is also found that there is an optimum calcination temperature for increasing the photo-induced hydrophilicity of the films. Fig. 9 shows the hydrophilization rate ($\Delta\theta$) in the first 10 min *versus* heat treatment temperature. The hydrophilization rate is highest for films treated at 700 °C. This may be due to the fact that the films calcined at 700 °C have the highest photocatalytic activity, which is beneficial for the photocatalytic decomposition of surface contami-

Table 3 Photocatalytic activity of TiO_2 and mesoporous TiO_2 thin films ($mTiO_2$) calcined at different temperatures[a]

Samples	Thickness /μm	Mass of film/mg	Degradation rate[b] (%)	Rate constant K/min^{-1}	Specific photoactivity 1[c] /mol g^{-1} h^{-1}	Specific photoactivity 2[d] /mol m^{-2} h^{-1}
$mTiO_2$/500 °C	0.15	7.4	7.9	1.2×10^{-3}	3.7×10^{-3}	2.0×10^{-3}
$mTiO_2$/700 °C	0.13	7.4	8.8	1.4×10^{-3}	4.1×10^{-3}	2.2×10^{-3}
$mTiO_2$/900 °C	0.12	7.4	Negligible[e]	Negligible	Negligible	Negligible
TiO_2/500 °C[f]	0.18	8.8	4.8	7.6×10^{-4}	1.9×10^{-3}	1.2×10^{-3}

[a] The area of quartz sheets covered with the $mTiO_2$ and TiO_2 layer is 140 cm^2. The coating cycle is 1. [b] Average degradation rate ($\Delta C/C_0$) of acetone after 1 h of photocatalytic reaction. [c] Acetone degradation per unit mass catalyst after 1 h of photocatalytic reaction. [d] Acetone degradation per unit film surface after 1 h of photocatalytic reaction. [e] Virtually no photoactivity. [f] Data from Table 5 of ref. 20.

nants. Moreover, the thin films heat treated at 700 °C possess a high surface hydroxyl content (compared with those calcined at 900 °C) and high degree of surface roughness (compared with films treated at 500 °C). Usually, the wettability of solid surfaces with water is governed not only by the chemical properties of a surfaces, but also by its geometry. As far as the geometry of a surface is concerned, the hydrophilic properties are enhanced by fine roughness. Therefore, an increase in surface roughness is a way to improve the hydrophilic properties. Of course, the chemical properties of the surface are another important factor affecting the hydrophilic properties. With an increase in chemisorbed –OH content on the surface, the polar properties and hydrophilicity of the surface are enhanced.[40] These factors (surface hydroxyl content and roughness) also result in a more rapid conversion of the surface to the super-hydrophilic state. After heat treatment at 900 °C, the films also show good photo-induced hydrophilicity, but no photoactivity. This further confirms that the mechanisms of photocatalytic activity and photo-induced superhydrophilicity are different. The hydrophilization rate was the slowest for samples calcined at 900 °C because these films have the lowest photocatalytic activity and surface hydroxyl content.

Fig. 10 shows the rate of hydrophobization ($\Delta\theta$) for samples stored in the dark for 7 days *versus* heat treatment temperature. The films calcined at 700 and 900 °C show the slowest and fastest conversion, respectively. The slow rate for the films treated at 700 °C is due to the fact that they not only have a high surface hydroxyl content (compared with those calcined at 900 °C), but also possess a greater degree of surface roughness (compared with films treated at 500 °C). Usually, surface hydroxyl groups and rough surface microstructures (or porous structures) favor the adsorption of water molecules and reduce the rate of the conversion from the hydrophilic to the hydrophobic state.[40] The lower hydrophobization rate of the films heat treated at 700 °C is considered to be the result of a synergetic effect between the surface hydroxyl groups and the surface roughness, *i.e.* the chemical properties and geometric characteristics of the surface. The TiO_2 film calcined at 900 °C exhibits the highest hydrophobization rate. This is because its surface hydroxyl content is the lowest, moreover, the density of rutile is greater than that of anatase and water evaporates more easily from larger pores.[40] These factors result in a higher conversion rate from the hydrophilic to the hydrophobic state.

Conclusions

The studies repoted above allow the following conclusions to be drawn. (1) The photocatalytic activity of mesoporous TiO_2 thin films is higher than that of conventional TiO_2 thin films due to the higher specific surface areas of the former and their mesoporous structures. (2) Mesoporous TiO_2 thin films calcined at 700 °C show the highest photocatalytic activity. This is attributed to the fact that these films are composed of both anatase and rutile phases. The transfer of photo-generated electrons from the anatase to the rutile phase may reduce the electron–hole combination rate and thus enhance the photoactivity. (3) Mesoporous TiO_2 films calcined at 700 °C show the best photo-induced hydrophilicity and the slowest conversion rate from the hydrophilic to the hydrophobic state. This is attributable to the results of the synergetic effect of good photocatalytic activity, sufficient surface hydroxyl content and surface roughness.

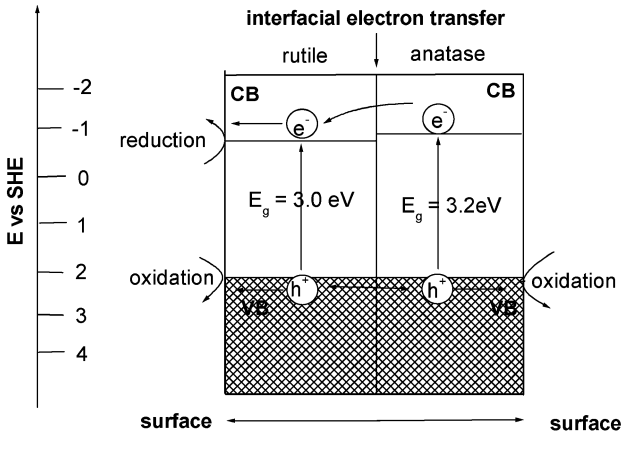

Fig. 7 Energy diagram for the heterogeneous anatase/rutile TiO_2 films at pH 7.

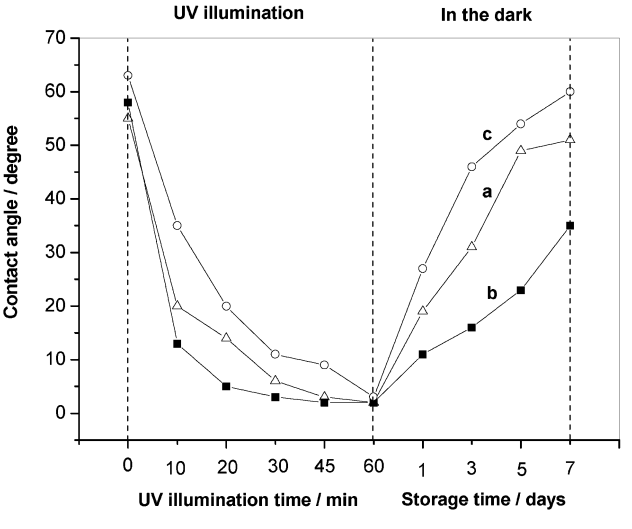

Fig. 8 Changes in the water contact angle of mesoporous TiO_2 thin films calcined at (a) 500, (b) 700 and (c) 900 °C when illuminated by UV light for 60 min and subsequently stored in a dark room for 7 days.

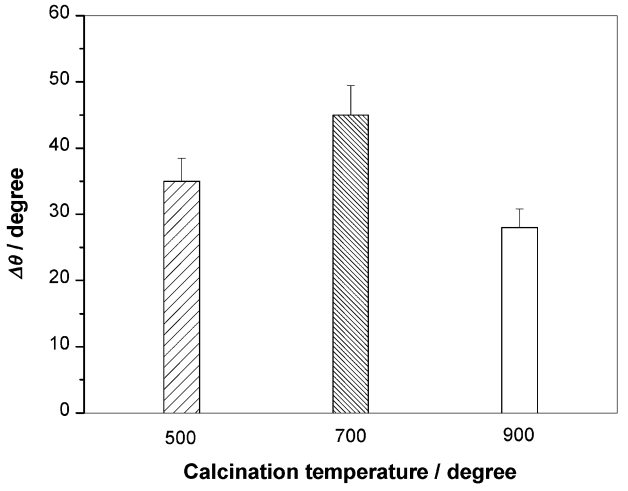

Fig. 9 Hydrophilization rate *versus* heat treatment temperature for mesoporous TiO_2 films. The rate of hydrophilization is approximated as the change in the water contact angle ($\Delta\theta$) in the first 10 min under 540 μW cm^{-2} UV illumination under ambient conditions (*i.e.* 295 K, RH: 50%, air).

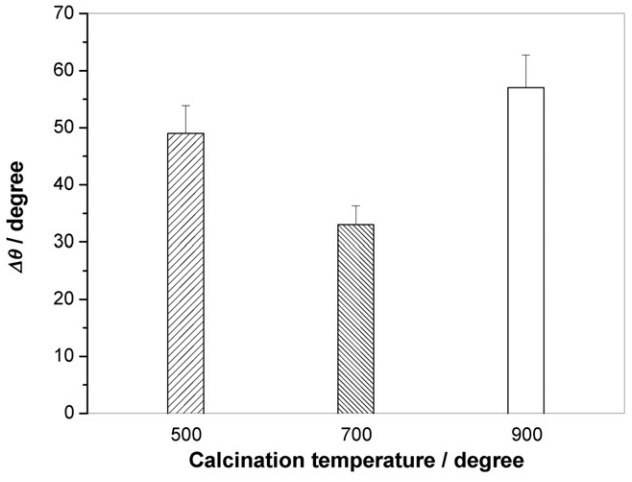

Fig. 10 Hydrophobization rate *versus* heat treatment temperature for mesoporous TiO_2 films. The rate of hydrophobization is approximated as the change in the water contact angle ($\Delta\theta$) after 7 days in the dark under ambient conditions (*i.e.* 295 K, RH: 50%, air).

Acknowledgements

The work described in this paper was partially supported by a grant from the National Natural Science Foundation of China and the Research Grants Council of the Hong Kong Special Administrative Region, China (project no. N_CUHK433/00). This work was also financially supported by the Foundation for University Key Teachers of the Ministry of Education, the National Natural Science Foundation of China (50072016). J. G. Y. expresses his sincere gratitude to the Postdoctoral Fellowships Scheme of The Chinese University of Hong Kong.

References

1 C. T. Kresge, M. E. Leonowicz, W. J. Roth, J. C. Vartuli and J. S. Beck, *Nature*, 1992, **359**, 710.
2 J. S. Beck, J. C. Vartuli, W. J. Roth, M. E. Leonowicz, C. T. Kresge, K. D. Schmitt, C. T. W. Chu, D. H. Olson, E. W. Sheppard, S. B. McCullen, J. B. Higgins and J. L. Schlenker, *J. Am. Chem. Soc.*, 1992, **114**, 10 834.
3 U. Ciesla, D. Demuth, R. Leon, P. M. Petroff, G. Stucky, K. Unger and F. Schuth, *J. Chem. Soc., Chem. Commun.*, 1994, 1387.
4 Q. Huo, D. I. Margoless, U. Cielsa, P. Feng, T. E. Gier, P. Sieger, R. Leon, P. M. Petroff, F. Schuth and G. Stucky, *Nature*, 1994, **368**, 317.
5 D. M. Antonelli and J. Y. Ying, *Angew. Chem., Int. Ed. Engl.*, 1995, **34**, 2014.
6 R. L. Putnam, N. Nakagawa, K. M. McGrath, N. Yao, I. A. Aksay, S. M. Gruner and A. Navrotsky, *Chem. Mater.*, 1997, **9**, 2690.
7 V. F. Stone and R. J. Davis, *Chem. Mater.*, 1998, **10**, 1468.
8 M. Thieme and F. Schuth, *Microporous Mesoporous Mater.*, 1999, **27**, 193.
9 M. A. Fox and M. T. Dulay, *Chem. Rev.*, 1993, **93**, 341.
10 M. Fujihira, Y. Satoh and T. Osa, *Nature*, 1981, **293**, 206.
11 P. A. M. Hotsenpiller, J. D. Bolt, W. E. Farneth, J. B. Lowekamp and G. S. Rohrer, *J. Phys. Chem. B*, 1998, **102**, 3216.
12 F. Gruy and M. Pijolat, *J. Am. Ceram. Soc.*, 1992, **75**, 657.
13 J. Retuert, R. Quijada and V. Arias, *Chem. Mater.*, 1998, **10**, 3923.
14 Q. Dai, N. Y. He, Y. Gao and C. W. Yuan, *Chem Lett.*, 1998, **11**, 1113.
15 P. D. Yang, D. Y. Zhao, D. I. Margolese, B. F. Chmelka and G. D. Stucky, *Nature*, 1998, **396**, 512.
16 D. M. Antonelli *Microporous Mesoporous Mater.*, 1999, **30**, 315.
17 Q. Dai, Z. L. Zhang, N. Y. He, P. Li and C. W. Yuan, *Mater. Sci. Eng., C*, 1999, **S8–9**, 417.
18 L. Saadoun, J. A. Ayllon, J. Jimenez-Becerril, J. Peral, X. Domenech and R. Rodriguez-Clemente, *Mater. Res. Bull.*, 2000, **35**, 193.
19 J. L. Zhang, M. Minagawa, M. Matsuoka, H. Yamashita and M. Anpo, *Catal. Lett.*, 2000, **66**, 241.
20 J. C. Yu, J. G. Yu and J. C. Zhao, *Appl. Catal., B*, 2002, **36**, 31.
21 J. C. Yu, J. G. Yu, W. K. Ho and L. Z. Zhang, *Chem. Commun.*, 2001, 1942.
22 J. C. Yu, J. G. Yu, W. K. Ho and L. Z. Zhang, *J. Photochem. Photobiol., A*, 2002in press.
23 J. C. Yu, L. Z. Zhang and J. G. Yu, *New J. Chem.*, 2002, **26**, 416.
24 Y. H. Yue, Z. Ma, W. M. Hua and Z. Gao, *Huaxue Xuebao*, 2000, **58**, 777.
25 P. D. Yang, D. Y. Zhao, D. I. Margolese, B. F. Chmelka and G. D. Stucky, *Chem. Mater.*, 1999, **11**, 2813.
26 E. P. Barrett, L. G. Joyner and P. H. Halenda, *J. Am. Chem. Soc.*, 1951, **73**, 373.
27 A. Fernandez, G. Lassaletta, V. M. Jimenez, A. Justo, A. R. Gonzalez-Elipe, J. M. Herrmann, H. Tahiri and Y. Ait-Ichou, *Appl. Catal., B.*, 1995, **7**, 49.
28 M. M. Rahman, K. M. Krishna, T. Soga, T. Jimbo and M. Umeno, *J. Phys. Chem. Solids*, 1999, **60**, 201.
29 H. Tang, K. Prasad, R. Sanjines, P. E. Schmid and F. Levy, *J. Appl. Phys.*, 1994, **75**, 2042.
30 J. G. Yu, J. C. Yu and X. J. Zhao, *J. Sol-Gel Sci. Technol.*, 2002, **24**, 95.
31 G. Lassaletta, A. Fernandez, J. P. Espinos and A. R. Gonzalez-Elipe, *J. Phys. Chem.*, 1995, **99**, 1484.
32 H. Zhang and J. F. Banfield, *J. Phys. Chem. B*, 2000, **104**, 3481.
33 A. Fujishima, T. N. Rao and D. A. Tryk, *J. Photochem. Photobiol., C*, 2000, **1**, 1.
34 H. Kominami, H. Kumamoto, Y. Kera and B. Ohtani, *Appl. Catal., B*, 2001, **30**, 329.
35 D. M. Shang and W. Y. Ching, *Phys. Rev. B*, 1995, **51**, 13 023.
36 L. Kruczynski, H. D. Gesser, C. W. Turner and E. A. Speers, *Nature*, 1981, **291**, 399.
37 A. L. Linsebigler, G. Lu and J. T. Yates, *Chem. Rev.*, 1995, **95**, 735.
38 M. Miyauchi, A. Nakajima, K. Hashimoto and T. Watanabe, *Adv. Mater.*, 2000, **12**, 1923.
39 N. Sakai, A. Fujishima, T. Watanabe and K. Hashimoto, *J. Phys. Chem. B*, 2001, **105**, 3023.
40 J. C. Yu, J. G. Yu, H. Y. Tang and L. Z. Zhang, *J. Mater. Chem.*, 2002, **12**, 81.